Chapter 13

Internal Waves

ABSTRACT
This chapter presents internal gravity waves, which exist in the presence of vertical stratification. After the derivation of the dispersion relation and examination of wave properties, the chapter briefly considers mountain waves and nonlinear effects. Vertical-mode decomposition is introduced and treated numerically as an eigenvalue problem.

13.1 FROM SURFACE TO INTERNAL WAVES

Starting at an early age, everyone has seen, experienced, and wondered about surface waves. Sloshing of water in bathtubs and kitchen sinks, ripples on a pond, surf at the beach, and swell further offshore are all manifestations of surface water waves. Sometimes we look at them with disinterest, and sometimes they fascinate us. But whatever our reaction or interest, their mechanism relies on a simple balance between gravity and inertia. When the surface of the water is displaced upward, gravity pulls it back downward, the fluid develops a vertical velocity (potential energy turns into kinetic energy), and because of inertia, the surface penetrates below its level of equilibrium. An oscillation results. A change in the phase of the oscillations from place to place causes the wave to travel. Because surface waves carry energy and no volume, they naturally occur wherever there is agitation that causes no overall water displacements, such as the shaking of a half-full bottle, the throwing of a stone in a pond, or a storm at sea.

The gravitational force continuously strives to restore the water surface to a horizontal level because water density is greater than that of the air above. It goes almost without saying that the same mechanism is at work whenever two fluid densities differ. This frequently occurs in the atmosphere when warm air overlies cold air; waves may then be manifested by cloud undulations, which may at times be remarkably periodic (Fig. 13.1). An oceanic example, known as the phenomenon of dead water (Fig. 1.4), is the occurrence of waves at the interface between an upper layer of relatively light water and a denser lower layer. Those waves, although unseen from the surface, can cause a sizable drag on a sailing vessel (Section 1.3).

Introduction to Geophysical Fluid Dynamics, Volume 101, ISSN 0074-6142, DOI: 10.1016/B978-0-12-088759-0.00013-4

FIGURE 13.1 Evidence of internal waves in the atmosphere. The presence of moisture causes condensation in the rising air (wave crests), thus revealing the internal wave as a periodic succession of cloud bands. (Photo by one of the authors, February 2005, Tassili N'Ajjer, Algeria)

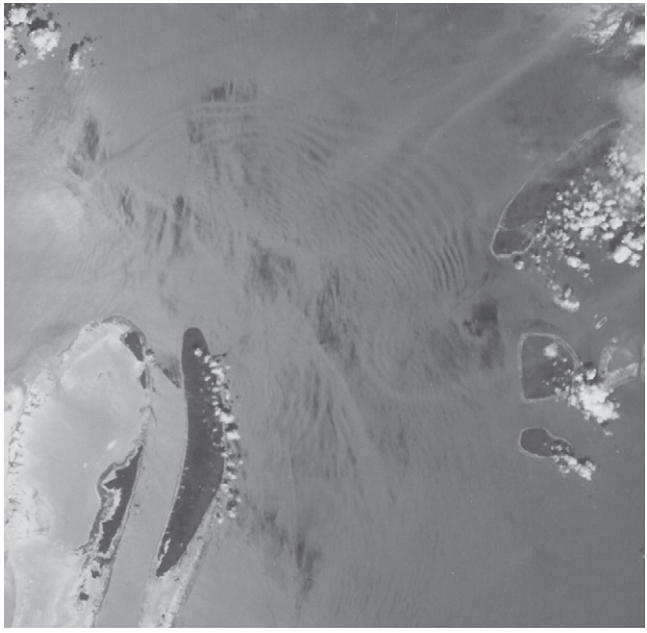

FIGURE 13.2 Surface manifestation of oceanic internal waves. The upward energy propagation of internal waves modifies the properties of surface waves rendering them visible from space. In this sunglint photograph taken from the space shuttle *Atlantis* on 19 November 1990 over Sibutu Passage in the Philippines (5°N, 119.5°E), a large group of tidally generated internal waves is seen to propagate northward into the Sulu Sea. (NASA Photo STS-38-084-060)

But the existence of such interfacial waves is not restricted to fluids with two distinct densities and a single interface. With three densities and two interfaces, two internal wave modes are possible; if the middle layer is relatively thin, the vertical excursions of the interfaces interact, letting energy pass from one level to the other. At the limit of a continuously stratified fluid, an infinite number of modes is possible, and wave propagation has both horizontal and vertical components (Fig. 13.2). Regardless of the level of apparent complexity in the wave pattern, the mechanism remains the same: There is a continuous interplay between gravity and inertia and a continuous exchange between potential and kinetic energies.

13.2 INTERNAL-WAVE THEORY

To study internal waves in their purest form, a few assumptions are necessary: There is no ambient rotation, the domain is infinite in all directions, there is no dissipative mechanism of any kind, and finally, the fluid motions and wave amplitudes are small. This last assumption is made to permit the linearization of the governing equations. However, we reinstate a term previously neglected, namely, the vertical acceleration term $\partial w/\partial t$ in the vertical momentum equation. We do so anticipating that vertical accelerations may play an important role in gravity waves. (Recall the discussion in Section 11.2 on the vertical oscillations of fluid parcels in a stratified fluid, which included the vertical acceleration). The inclusion of this term breaks the hydrostatic balance, but so be it! Finally, we decompose the fluid density as follows:

$$\text{Actual fluid density} = \rho_0 + \bar{\rho}(z) + \rho'(x, y, z, t), \tag{13.1}$$

where ρ_0 is the reference density (a pure constant), $\bar{\rho}(z)$ is the ambient equilibrium stratification, and $\rho'(x, y, z, t)$ is the density fluctuation induced by the wave (lifting and lowering of the ambient stratification). The inequality $|\bar{\rho}| \ll \rho_0$ is enforced to justify the Boussinesq approximation (Section 3.7), whereas the further inequality $|\rho'| \ll |\bar{\rho}|$ is required to linearize the wave problem. The total pressure field is decomposed in a similar manner. With the preceding assumptions, the governing equations become (Section 4.4)

$$\frac{\partial u}{\partial t} = -\frac{1}{\rho_0}\frac{\partial p'}{\partial x} \tag{13.2a}$$

$$\frac{\partial v}{\partial t} = -\frac{1}{\rho_0}\frac{\partial p'}{\partial y} \tag{13.2b}$$

$$\frac{\partial w}{\partial t} = -\frac{1}{\rho_0}\frac{\partial p'}{\partial z} - \frac{1}{\rho_0} g\rho' \tag{13.2c}$$

$$\frac{\partial u}{\partial x} + \frac{\partial v}{\partial y} + \frac{\partial w}{\partial z} = 0 \tag{13.2d}$$

$$\frac{\partial \rho'}{\partial t} + w\frac{\mathrm{d}\bar{\rho}}{\mathrm{d}z} = 0. \tag{13.2e}$$

The factor $\mathrm{d}\bar{\rho}/\mathrm{d}z$ in the last term can be transformed by introducing the stratification frequency (Brunt–Väisälä frequency) defined earlier in Eq. (11.3):

$$N^2 = -\frac{g}{\rho_0}\frac{\mathrm{d}\bar{\rho}}{\mathrm{d}z}. \tag{13.3}$$

For simplicity, we will assume it to be uniform over the extent of the fluid. This corresponds to a linear density variation in the vertical. Because all coefficients in the preceding linear equations are constant, a wave solution of the form

$$\mathrm{e}^{\mathrm{i}(k_x x + k_y y + k_z z - \omega t)}$$

is sought. Transformation of the derivatives into products (e.g., $\partial/\partial x$ becomes $\mathrm{i}k_x$) leads to a 5-by-5 homogeneous algebraic problem. The solution is nonzero if the determinant vanishes, and this requires that the wave frequency ω be given by

$$\omega^2 = N^2 \frac{k_x^2 + k_y^2}{k_x^2 + k_y^2 + k_z^2} \tag{13.4}$$

in terms of the wavenumbers, k_x, k_y, and k_z, and the stratification frequency, N. This is the dispersion relation of internal gravity waves.

A number of wave properties can be stated by examination of this relation. First and foremost, it is obvious that the numerator is always smaller than the denominator, meaning the wave frequency will never exceed the stratification frequency; that is,

$$\omega \leq N \tag{13.5}$$

for positive frequencies. The reason for this upper bound can be traced back to the presence of the vertical acceleration term in Eq. (13.2c). Indeed, without that term the denominator in Eq. (13.4) reduces from $k_x^2 + k_y^2 + k_z^2$ to only k_z^2, implying that the nonhydrostatic term may be neglected as long as $k_z^2 + k_y^2 \ll k_z^2$. This occurs for waves with horizontal wavelengths much longer than their vertical wavelengths; the frequency of those waves is much less than N. For progressively shorter waves, the correction becomes increasingly important, the frequency rises but saturates at the value N. We may then ask what would happen if we agitate a stratified fluid at a frequency greater than its own stratification frequency. The answer is that with such short periods, fluid particles do not have the time to oscillate at their natural frequency and instead follow whatever displacements are forced on them; the disturbance turns into a local patch of turbulence, and no energy is carried away by waves. Using a neutrally buoyant float in the ocean, D'Asaro and Lien (2000) have shown that in stratified waters values of ω/N in the range 0.2–1 generally correspond to internal waves, whereas, at the same places, values above 1 ($1 < \omega/N < 50$) correspond to turbulent fluctuations.

Another important property derived from the dispersion relation (13.4) is that the frequency does not depend on the wavenumber magnitude (and thus on the wavelength) but only on its angle with respect to the horizontal plane. Indeed, with $k_x = k\cos\theta\cos\phi$, $k_y = k\cos\theta\sin\phi$, and $k_z = k\sin\theta$, where $k = \left(k_x^2 + k_y^2 + k_z^2\right)^{1/2}$ is the wavenumber magnitude, θ is its angle from the horizontal (positive or negative), and ϕ is the angle of its horizontal projection with the x–axis, we obtain

$$\omega = \pm N\cos\theta, \tag{13.6}$$

proving that the frequency depends only on the pitch of the wavenumber and, of course, the stratification frequency. The fact that two signs are allowed indicates that the wave can travel in one of two directions, upward or downward along the wavenumber direction. On the other hand, if the frequency is imposed (e.g., by tidal forcing), all waves regardless of wavelength propagate at fixed angles from the horizontal. The lower the frequency, the steeper the direction. At the limit of very low frequencies, the phase propagation is purely vertical ($\theta = 90^\circ$).

13.3 STRUCTURE OF AN INTERNAL WAVE

Let us rotate the x and y axes so that the wavenumber vector is contained in the (x, z) vertical plane (i.e., $k_y = 0$, and there is no variation in the y-direction and no v velocity component). The expressions for the remaining two velocity components and the density fluctuation are

$$u = -A\,\frac{g\omega k_z}{N^2 k_x}\sin(k_x x + k_z z - \omega t) \tag{13.7a}$$

$$w = +A\,\frac{g\omega}{N^2}\sin(k_x x + k_z z - \omega t) \tag{13.7b}$$

$$p' = -A\,\frac{\rho_0 g k_z}{k_x^2 + k_z^2}\sin(k_x x + k_z z - \omega t) \tag{13.7c}$$

$$\rho' = +A\rho_0\cos(k_x x + k_z z - \omega t). \tag{13.7d}$$

For k_x, k_z, and ω all positive, the structure of the wave is depicted on Fig. 13.3. The areas of upwelling (crests) and downwelling (troughs) alternate both horizontally and vertically, and lines of constant phase (e.g., following crests) tilt perpendicularly to the wavenumber vector. The trigonometric functions in solution (13.7) tell us that the phase $k_x x + k_z z - \omega t$ remains constant with time if one translates in the direction (k_x, k_z) of the wavenumber at the speed (see Appendix B):

$$c = \frac{\omega}{\sqrt{k_x^2 + k_z^2}}. \tag{13.8}$$

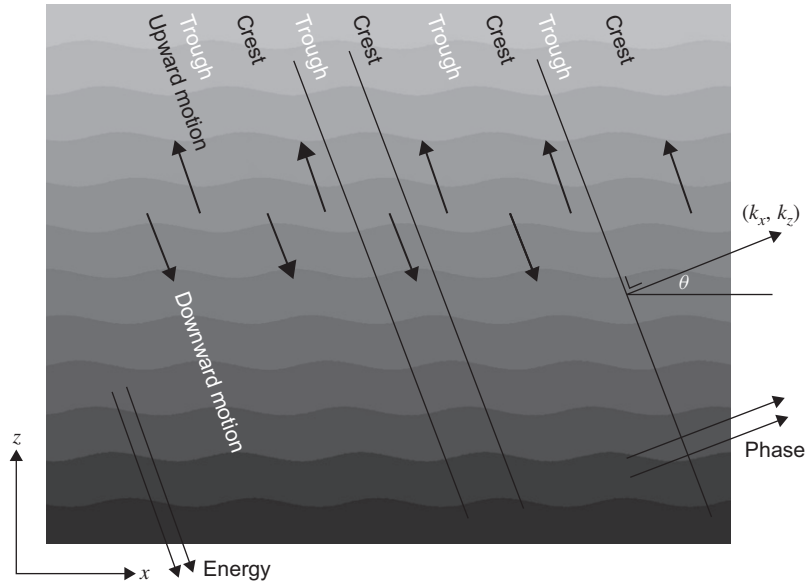

FIGURE 13.3 Vertical structure of an internal wave.

This is the phase speed, at which lines of crests and troughs translate. Because the velocity components, u and w, are in quadrature with the density fluctuations, the velocity is nil at the crests and troughs but is maximum a quarter of a wavelength away. The signs indicate that when one component is positive, the other is negative, implying downwelling to the right and upwelling to the left as indicated in Fig. 13.3. The ratio of velocities $(-k_x/k_z)$ further indicates that the flow is everywhere perpendicular to the wavenumber vector and thus parallel to the lines connecting crests and troughs. Internal waves are transverse waves. A comparison of the signs in the expressions of w and ρ' reveals that rising motions occur ahead of crests and sinking motions occur ahead of troughs, eventually forming the next crests and troughs, respectively. Thus, the wave moves forward and, because of the inclination of its wavenumber, also upward.

The propagation of the energy is given by the group velocity, which is the gradient of the frequency with respect to the wavenumber (Appendix B):

$$c_{gx} = \frac{\partial \omega}{\partial k_x} = +\frac{\omega k_z^2}{k_x\left(k_x^2 + k_z^2\right)} \tag{13.9}$$

$$c_{gz} = \frac{\partial \omega}{\partial k_z} = -\frac{\omega k_z}{\left(k_x^2 + k_z^2\right)}. \tag{13.10}$$

The direction is perpendicular to the wavenumber (k_x, k_z) and is downward. Thus, although crests and troughs appear to move upward, the energy actually sinks. The reader can verify that irrespective of the signs of the frequency and wavenumber components, the phase and energy always propagate in the same horizontal direction (though not at the same rates) and in opposite vertical directions.

Let us now turn our attention to the extreme cases. The first one is that of a purely horizontal wavenumber ($k_z = 0$, $\theta = 0$). The frequency is then N, and the phase speed is N/k_x. The absence of wave-like behavior in the vertical direction implies that all crests and troughs are vertically aligned. The motion is strictly vertical, and the group velocity vanishes, implying that the energy does not travel. The opposite extreme is that of a purely vertical wavenumber ($k_x = 0$, $\theta = 90°$). The frequency vanishes, implying a steady state. There is then no wave propagation. The velocity is purely horizontal and, of course, laterally uniform. The picture is that of a stack of horizontal sheets each moving, without distortion, with its own speed and in its own direction. If a boundary obstructs the flow at some depth, none of the fluid at that depth, however remote from the obstacle, is allowed to move. This phenomenon, occurring at very low frequencies in highly stratified fluids, is none other than the blocking phenomenon discussed at the end of Section 11.5 and presented as the stratified analogue of the Taylor column in rotating fluids.

In stratified and rotating fluids, the lowest possible internal-wave frequency is not zero but the inertial frequency f (see Analytical Problem 13.3). At that limit, the wave motion assumes the form of inertial oscillations, wherein fluid parcels execute horizontal circular trajectories (Section 2.3). Such limiting behavior is an attribute of inertia-gravity waves in homogeneous rotating fluids (Section 9.3) and is not surprising, since internal waves in stratified rotating fluids are the three-dimensional extensions of the inertia-gravity waves of homogeneous rotating fluids.

13.4 VERTICAL MODES AND EIGENVALUE PROBLEMS

Up to now, we considered internal waves in the rather schematic situation of an unbounded, nonrotating domain of uniform stratification. This is tantamount to considering only waves of wavelength much shorter than both the domain size and the length over which N^2 varies, and of frequency sufficiently high not to be influenced by the earth's rotation.

If we look at actual vertical profiles of density and their associated stratification frequencies (Fig. 13.4, for example), it is clear that stratification is far from uniform in the vertical, and we should question the validity of the preceding theory, except for very short vertical wavelengths. What happens then to internal waves with wavelengths comparable to the scale over which stratification changes?

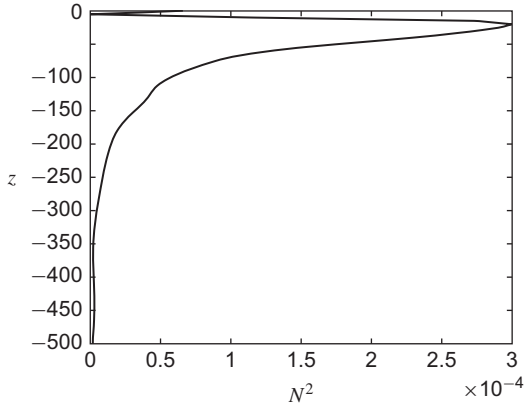

FIGURE 13.4 Stratification frequency squared (N^2 in s^{-2}) obtained from averaged climatological density profile in the Western Mediterranean Sea. (Data from Medar©)

To answer this question with a relatively simple analysis, we assume constant depth and eliminate surface waves by imposing a rigid lid (Sections 7.5 and 12.2). In return, we reinstate rotation by invoking the f-plane approximation. Because it is typically the case in nature, we assume that $f^2 < N^2(z)$ holds everywhere across the fluid column, that is,

$$N^2(z) = -\frac{g}{\rho_0}\,\frac{\mathrm{d}\bar{\rho}}{\mathrm{d}z} > f^2 > 0. \tag{13.11}$$

Within this framework, the equations governing small perturbations are now

$$\frac{\partial u}{\partial t} - fv = -\frac{1}{\rho_0}\,\frac{\partial p'}{\partial x} \tag{13.12a}$$

$$\frac{\partial v}{\partial t} + fu = -\frac{1}{\rho_0}\,\frac{\partial p'}{\partial y} \tag{13.12b}$$

$$\frac{\partial w}{\partial t} = -\frac{1}{\rho_0}\,\frac{\partial p'}{\partial z} - \frac{g}{\rho_0}\,\rho' \tag{13.12c}$$

$$\frac{\partial u}{\partial x} + \frac{\partial v}{\partial y} + \frac{\partial w}{\partial z} = 0 \tag{13.12d}$$

$$\frac{\partial \rho'}{\partial t} + w\,\frac{\mathrm{d}\bar{\rho}}{\mathrm{d}z} = 0. \tag{13.12e}$$

As for pure internal waves, we do not make use of the hydrostatic approximation. For a uniform topography, we can apply the technique of separation of

variables and search for solutions of the type:

$$u = \mathcal{F}(z)\,\mathcal{U}(x,y)\,\mathrm{e}^{-\mathrm{i}\omega t} \tag{13.13a}$$

$$v = \mathcal{F}(z)\,\mathcal{V}(x,y)\,\mathrm{e}^{-\mathrm{i}\omega t} \tag{13.13b}$$

$$p' = \rho_0 \mathcal{F}(z)\,\mathcal{P}(x,y)\,\mathrm{e}^{-\mathrm{i}\omega t} \tag{13.13c}$$

$$w = \mathrm{i}\omega \mathcal{W}(z)\,\mathcal{P}(x,y)\,\mathrm{e}^{-\mathrm{i}\omega t} \tag{13.13d}$$

$$\rho' = -N^2 \frac{\rho_0}{g} \mathcal{W}(z)\,\mathcal{P}(x,y)\,\mathrm{e}^{-\mathrm{i}\omega t}. \tag{13.13e}$$

Using these expressions in the governing equations (13.12), we realize that Eq. (13.12e) is already satisfied and that the four remaining equations reduce to

$$-\mathrm{i}\omega\,\mathcal{U} = f\mathcal{V} - \frac{\partial \mathcal{P}}{\partial x} \tag{13.14a}$$

$$-\mathrm{i}\omega\,\mathcal{V} = -f\mathcal{U} - \frac{\partial \mathcal{P}}{\partial y} \tag{13.14b}$$

$$\left(\omega^2 - N^2\right)\mathcal{W} = -\frac{\mathrm{d}\mathcal{F}}{\mathrm{d}z} \tag{13.14c}$$

$$\frac{1}{\mathcal{P}}\left(\frac{\partial \mathcal{U}}{\partial x} + \frac{\partial \mathcal{V}}{\partial y}\right) = -\mathrm{i}\,\frac{\omega}{\mathcal{F}}\,\frac{\mathrm{d}\mathcal{W}}{\mathrm{d}z}. \tag{13.14d}$$

The first two equations do not depend on z, the third one depends on neither x or y, while the last equation has a left-hand side that does not depend on z and a right-hand side that does not depend on x and y. This last equation can only be met if both terms are constant. For dimensional reasons, we call this constant $\mathrm{i}\omega/gh^{(j)}$, where $h^{(j)}$ has the dimension of a depth and is commonly called the *equivalent depth*. The reason for this label will become clear shortly.

Substitution of the right-hand side of Eq. (13.14d),

$$-\mathrm{i}\,\frac{1}{\mathcal{F}}\,\frac{\mathrm{d}\mathcal{W}}{\mathrm{d}z} = \frac{\mathrm{i}}{gh^{(j)}},$$

into the z-dependent equation (13.14c) leads to an equation governing the vertical mode $\mathcal{W}(z)$:

$$\frac{\mathrm{d}^2\mathcal{W}}{\mathrm{d}z^2} + \frac{\left(N^2 - \omega^2\right)}{gh^{(j)}}\,\mathcal{W} = 0, \tag{13.15}$$

while the horizontal structure $\mathcal{U}$, $\mathcal{V}$, $\mathcal{P}$ is solution of Eqs. (13.14a) and (13.14b) completed with the result of Eq. (13.14d):

$$\frac{\partial \mathcal{U}}{\partial x} + \frac{\partial \mathcal{V}}{\partial y} = \frac{\mathrm{i}\omega}{gh^{(j)}}\,\mathcal{P}. \tag{13.16}$$

These three equations possess the same structure as the shallow-water wave equations with constant depth (Section 9.1). We observe that the surface elevation η is replaced by $\mathcal{P}/g$ and the depth h by $h^{(j)}$. Therefore, we can immediately recover the wave solutions of the shallow-water theory and verify that for a horizontal periodic solution of the type $(\mathcal{U}, \mathcal{V}, \mathcal{P}) = (U, V, P)\mathrm{e}^{\mathrm{i}(k_x x + k_y y)}$ with constant coefficients U, V and P, these waves obey the dispersion relation of inertial (Poincaré) waves:

$$\omega^2 = f^2 + gh^{(j)}\left(k_x^2 + k_y^2\right). \tag{13.17}$$

For horizontally finite domains, only discrete values of (k_x, k_y) pairs are allowed, but we will not explore this possibility here, preferring to consider the pair (k_x, k_y) as given.

13.4.1 Vertical Eigenvalue Problem

Now that we know the horizontal structure of the wave, we have to find its associated vertical structure. This can be done by substituting the horizontal dispersion relation (13.17) in the vertical-mode equation (13.15), which leads to the following problem:

$$\frac{\mathrm{d}^2\mathcal{W}}{\mathrm{d}z^2} + \left(k_x^2 + k_y^2\right)\frac{N^2(z) - \omega^2}{\omega^2 - f^2}\,\mathcal{W} = 0, \tag{13.18}$$

with boundary conditions

$$\mathcal{W} = 0 \quad \text{at } z = 0 \text{ and } z = H \tag{13.19}$$

corresponding to rigid lid on top and flat bottom below.

We are in the presence of a homogeneous differential equation with homogeneous boundary conditions, that is, the solution is trivially $\mathcal{W} = 0$ unless ω assumes a special value. As it turns out, there exists a whole series of special ω values for which $\mathcal{W}$ may be nonzero. These are called eigenvalues, and the corresponding $\mathcal{W}(z)$ solutions are called eigenfunctions or, more specifically in our case, *vertical modes*.

13.4.2 Bounds on Frequency

We anticipate that there should be some bounds on the wave frequencies as we are already aware of $\omega^2 < N^2$ from Section 13.2. In order to find these bounds, we apply an integral technique similar to that used to analyze stability of shear flows (Section 10.2).

When we multiply Eq. (13.18) by the complex conjugate $\mathcal{W}^*$, integrate vertically across the domain, perform an integration by part on the first term,

and use boundary conditions (13.19), we obtain

$$\int_0^H \left|\frac{\mathrm{d}\mathcal{W}}{\mathrm{d}z}\right|^2 \mathrm{d}z = \left(k_x^2+k_y^2\right)\int_0^H \frac{N^2-\omega^2}{\omega^2-f^2}\,|\mathcal{W}|^2\,\mathrm{d}z. \tag{13.20}$$

For $f^2 < N^2$, the common situation, and as long as ω is real, it is clear that only values within the range

$$f^2 \le \omega^2 \le N^2_{\max} \tag{13.21}$$

are permitted, since outside this range the right-hand side of Eq. (13.20) would be negative and unable to match the positive left-hand side.

However, we can ask whether there could be complex values of ω. First, a purely imaginary solution is not possible since $\omega = \mathrm{i}\omega_i$ would make the right-hand side of Eq. (13.20) always negative.[1] In the general case $\omega = \omega_r + \mathrm{i}\omega_i$, it is sufficient to consider the imaginary part of the fraction in Eq. (13.20):

$$\Im\left(\frac{N^2-\omega^2}{\omega^2-f^2}\right) = -2\omega_r\omega_i\,\frac{N^2-f^2}{(\omega_r^2-\omega_i^2-f^2)^2+4\omega_r^2\omega_i^2} \tag{13.22}$$

and to realize that any $\omega_i \neq 0$ prevents Eq. (13.20) from being met because its real left-hand side cannot match its nonreal right-hand side. Therefore, it is true that Eq. (13.20) allows only real ω.

In conclusion, for $f^2 < N^2$, we find pure wave motions with frequencies in the range (13.21). Compared to Eq. (13.5), we see that one effect of rotation is to eliminate the lower frequencies. We also note that, as many times before, if a wave of frequency ω exists, so does one of frequency $-\omega$, corresponding to propagation in the opposite direction.

13.4.3 Simple Example of Constant N^2

We can solve analytically the case of uniform stratification in a rotating bounded domain. The eigenvalue problem has the following immediate solution

$$\mathcal{W}(z) = \sin k_z z, \quad k_z = j\frac{\pi}{H}, \quad j = 1, 2, 3, \ldots \tag{13.23}$$

with the accompanying dispersion relation

$$\omega^2 = \frac{\left(k_x^2+k_y^2\right)N^2 + k_z^2 f^2}{k_x^2+k_y^2+k_z^2}. \tag{13.24}$$

[1] We assumed from the beginning $0 \le f^2 \le N^2$, but the interested reader could analyze the case $N^2 < 0$, corresponding to gravitational instability. In this case, complex ω values are possible as we can expect on physical ground.

Due to the finiteness of the vertical domain size, the vertical wavenumber k_z now takes discrete values, and the corresponding functions $\mathcal{W}(z)$ form a discrete set of eigenfunctions. Yet, we have an infinite number of them as predicted in Section 12.4. We can verify that all frequencies fall in the range (13.21) and recognize that the spatial structures are the same as in the unbounded domain, except that only those wavelengths are permitted that satisfy the boundary conditions.

Likewise, the constant $gh^{(j)}$, which had been free sofar, may only take one among a discrete set of values:

$$gh^{(j)} = \frac{\omega^2 - f^2}{k_x^2 + k_y^2} = \frac{N^2 - f^2}{k_x^2 + k_y^2 + \left(j\frac{\pi}{H}\right)^2}. \tag{13.25}$$

Since $gh^{(j)}$ plays here the same role in the horizontal structure of each mode as gH did in a shallow-water system, we can form an analogous radius of deformation.

$$R_j = \frac{\sqrt{gh^{(j)}}}{f}. \tag{13.26}$$

This *internal* radius of deformation plays the same role as the *external* radius of deformation did in the shallow water system. Among other properties, it characterizes the horizontal scale at which both rotation and gravity, here through stratification, come into play, and, for example, the lateral trapping scale of an internal coastal Kelvin wave is the internal deformation radius (see Analytical Problem 13.9).

By virtue of $\omega^2/f^2 = 1 + (k_x^2 + k_y^2)\, R_j^2$, waves with a shorter wavelength than the deformation radius are influenced primarily by stratification, while those with longer scales are dominated by rotation. The radius of deformation is thus the scale at which rotation and stratification play equally significant roles. Note that it varies from mode to mode, with higher modes having shorter radii. Waves that vary rapidly in the vertical ($j \gg 1$) have a shorter radius of deformation, subjecting them to stronger rotational effects than waves with smoother vertical variation.

For small aspect ratios $k_x^2 + k_y^2 \ll k_z^2$ with strong stratification $f^2 \ll N^2$, the expression of the deformation radius reduces to

$$R_j \simeq \frac{NH}{j\pi f}, \quad j = 1, 2, 3, \ldots \tag{13.27}$$

The uniform-stratification application has the advantage of showing how rotation and finite domain influence the wave dispersion relation compared to Eq. (13.4), but it is inadequate to determine the eigenfrequencies of a system with highly nonuniform stratification, such as one with a localized pycnocline.

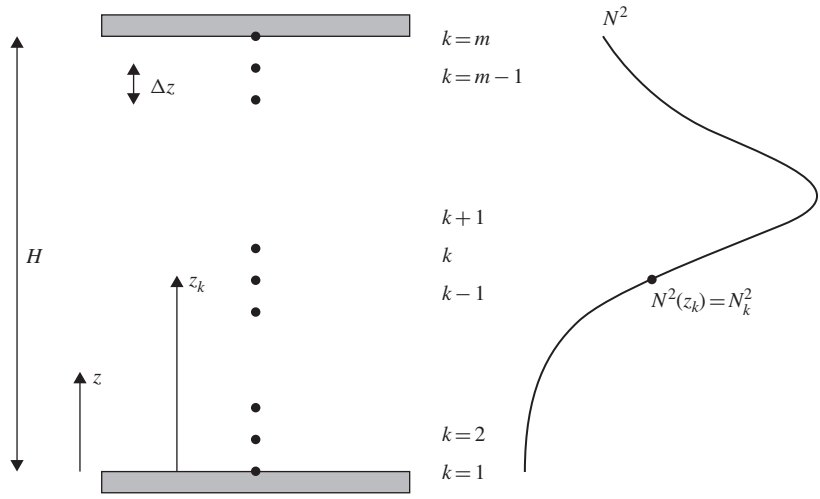

FIGURE 13.5 Notation for the discretization in search of vertical modes.

Although analytical asymptotic methods[2] exist to tackle such an eigenvalue problem, it is generally easier and more accurate to resort to numerical methods. This is even more true if the system to be analyzed is a concrete one, where the density profile was measured or obtained from climatological databases with data at discrete vertical levels.

13.4.4 Numerical Decomposition into Vertical Modes

The discretization chosen here is a straightforward finite-difference technique. For the sake of simplicity, uniform grid spacing Δz is assumed. The first and last grid points are chosen, respectively, on the flat bottom and at the rigid lid (Fig. 13.5), since boundary conditions on the unknown itself are imposed there. The discretized field w of the exact solution $\mathcal{W}$ at location z_k is noted w_k so that the discretization reads

$$\mathrm{w}_{k+1}+\mathrm{w}_{k-1}-2\,\mathrm{w}_k+\Delta z^2\left(k_x^2+k_y^2\right)\frac{N^2(z_k)-\omega^2}{\omega^2-f^2}\,\mathrm{w}_k=0,\quad k=2,3,\ldots,m-1 \tag{13.28}$$

$$\text{with}\quad \mathrm{w}_1=0,\quad \mathrm{w}_m=0. \tag{13.29}$$

This problem can be recast in matrix form by collecting all w_k into an array $\mathbf{w}$:

$$\mathbf{A}(\omega^2)\mathbf{w}\;=\;0, \tag{13.30}$$

[2] See WKB methods in Bender and Orszag (1978).

where the matrix **A** is tridiagonal (as it was for the diffusion problem, see Section 5.5) and depends on ω^2. The possible ω frequencies are then those that allow a nonzero **w**, and this can only occur if the system is singular, that is,

$$\det(\mathbf{A}) = 0. \tag{13.31}$$

The problem then reduces to finding the zeros of the determinant of **A**. For each value of ω^2 for which the determinant vanishes, the corresponding discretized spatial eigenmode **w** is the solution of Eq. (13.30). In linear algebra, finding this vector for a given singular matrix is a standard problem and amounts to finding the null-space of matrix **A**. The solution of our problem can therefore be obtained by searching those values of ω^2 for which the determinant of **A** is zero and then using a linear algebra package to determine the null-space associated with the now singular matrix to retrieve the discretized vertical structure of the internal wave.

However, finding the zeros of a complicated function is not a trivial task, and we risk to miss some zeros, even if the theoretical bounds Eq. (13.21) for ω^2 can guide the search algorithm. We can neither be sure that numerical solutions of Eq. (13.31) fall into the same range, although those falling clearly outside should certainly qualify as nonphysical.

To isolate the variable ω^2, we reformulate the problem (13.30) by restating it as

$$-\frac{\omega^2}{f^2}\left[-\mathrm{w}_{k+1}-\mathrm{w}_{k-1}+(2+\epsilon)\,\mathrm{w}_k\right]+\left[-\mathrm{w}_{k+1}-\mathrm{w}_{k-1}+\left(2+\epsilon N_k^2 f^{-2}\right)\mathrm{w}_k\right]=0 \tag{13.32}$$

with $\epsilon = \Delta z^2\left(k_x^2+k_y^2\right) > 0$. Values of k are limited to $2 \le k \le m-1$ since the boundary conditions are readily implemented. Equation (13.32) can be written as a linear problem:

$$\mathbf{B}\mathbf{w} = \lambda \mathbf{C}\mathbf{w}, \quad \lambda = \frac{\omega^2}{f^2} \tag{13.33}$$

where matrices **B** and **C** are tridiagonal and, most importantly, independent of ω^2. Both matrices also have -1 on their subdiagonal and superdiagonal lines, whereas the diagonal of **C** repeats $2+\epsilon$ and that of **B**, $2+\epsilon N_k^2/f^2$. Further, **B** and **C** are symmetric positive definite since they are diagonally dominant.

Equation (13.33) is stated as a standard linear algebra problem (called generalized eigenvalue problem) for which solvers and theorems exist (e.g., the Rayleigh–Ritz inequalities that are the subject of Numerical Exercise 13-2).

We can recast the problem in an even more familiar form by noting that for any positive definite matrix, its inverse exists, and therefore, by defining $\tilde{\mathbf{w}} = \mathbf{C}\mathbf{w}$, we recover a standard eigenvalue problem

$$\mathbf{A}\tilde{\mathbf{w}} = \lambda\tilde{\mathbf{w}} \qquad \text{with} \qquad \mathbf{A} = \mathbf{B}\mathbf{C}^{-1}. \tag{13.34}$$

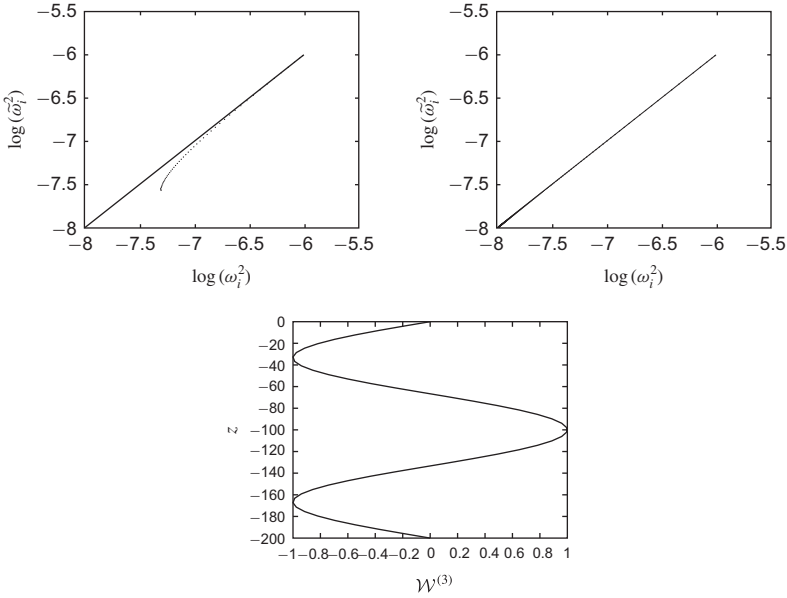

FIGURE 13.6 Numerical estimation $\log\left(\tilde{\omega_j}^2\right)$ versus exact value $\log\left(\omega_j^2\right)$ of internal-mode frequencies, using 50 (top left panel) and 450 (top right panel) discrete levels in the vertical. Bottom panel: Numerical profile of the third vertical mode, clearly corresponding to $\sin(3\pi z/H)$.

Once the eigenvalues λ and eigenvectors $\tilde{\mathbf{w}}$ are found, the discretized physical mode $\mathbf{w}$ can be reconstructed by means of $\mathbf{w} = \mathbf{C}^{-1}\tilde{\mathbf{w}}$.

We can be assured that the problem has only real solutions. Since both $\mathbf{B}$ and $\mathbf{C}$ are symmetric positive definite, multiplying Eq. (13.33) for a given eigenvalue λ_j and eigenvector $\mathbf{w}^j$ by the transposed complex conjugate $\mathbf{w}^{j*}$ reveals[3] that λ_j must be real for any j.

We note that, contrary to the analytical solution for which an infinite number of modes exist, only a finite number $(m-2)$ of eigenvalues and modes can be calculated in the discretized version.

To verify the numerical method outlined above, we calculate the numerical solution for the case of uniform N^2 and compare it with the known analytical solution Eq. (13.23)–(13.24). As expected, the largest eigenvalues, those corresponding the longest vertical wavelengths, are well represented, even for a moderate number of grid points (Fig. 13.6). However, the frequencies closer to f require finer resolution because of their shorter wavelengths. To represent mode j accurately, we indeed need a spacing $j\Delta z \ll H$.

[3]We use the fact that both $\mathbf{w}^{j*}\mathbf{B}\mathbf{w}^j$ and $\mathbf{w}^{j*}\mathbf{C}\mathbf{w}^j$ are real because of the positive definite nature of $\mathbf{B}$ and $\mathbf{C}$.

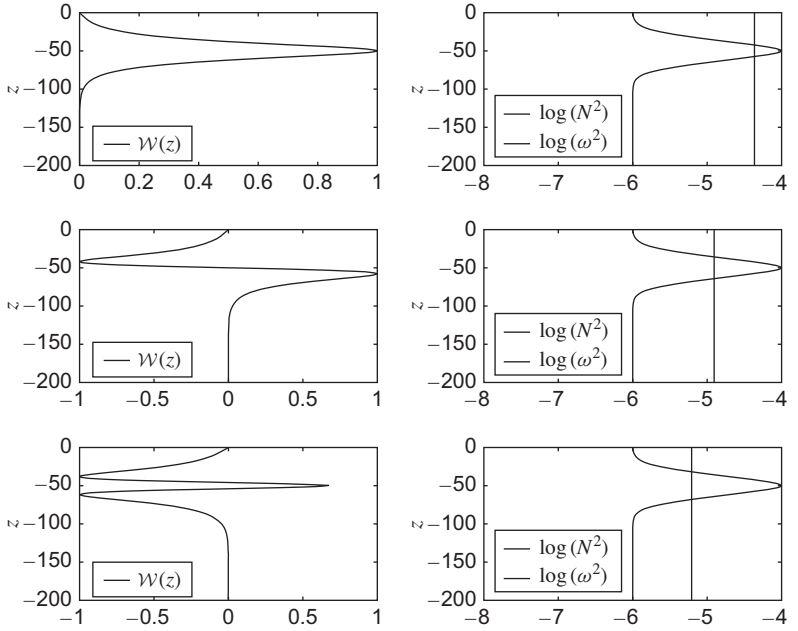

FIGURE 13.7 First three modes (left panel) of a nonuniform stratification with N^2 peak. The corresponding values of ω^2 are set against the N^2 profile in the right panel. Note that the ω^2 values lie between the extrema of N^2.

13.4.5 Waves Concentration at a Pycnocline

The numerical method shown above is now being used to analyze a situation in which the N^2 profile exhibits a maximum, which corresponds to a region of greater density variation, that is, a pycnocline. To do so, we take a schematic density profile (Figure 13.7), with a stratification frequency varying between N_0 and N_1 such that $f^2 < N_0^2 < N^2(z) < N_1^2$.

The first three modes (Fig. 13.7), correspond to the highest frequencies, and their vertical profiles (left panels) indicate a concentration of amplitude and highest gradients in the vicinity of the peak of $N^2(z)$, the pycnocline. This can be understood in the light of the sign of $(N^2-\omega^2)/(f^2-\omega^2)$ that appears in Eq. (13.18). Where this factor is positive, the eigenfunctions are oscillatory in nature and where it is negative, they exhibit exponential decay. Since the term changes sign within the domain because $N_0^2 < \omega^2 < N_1^2$ (see right panels of Fig. 13.7), the solution switches from oscillations in regions of $\omega^2 \leq N^2$ to exponential behavior elsewhere, decreasing toward zero at the boundaries of the domain. A point where $\omega^2 = N^2$ is called a *turning point*. With ω^2 cutting

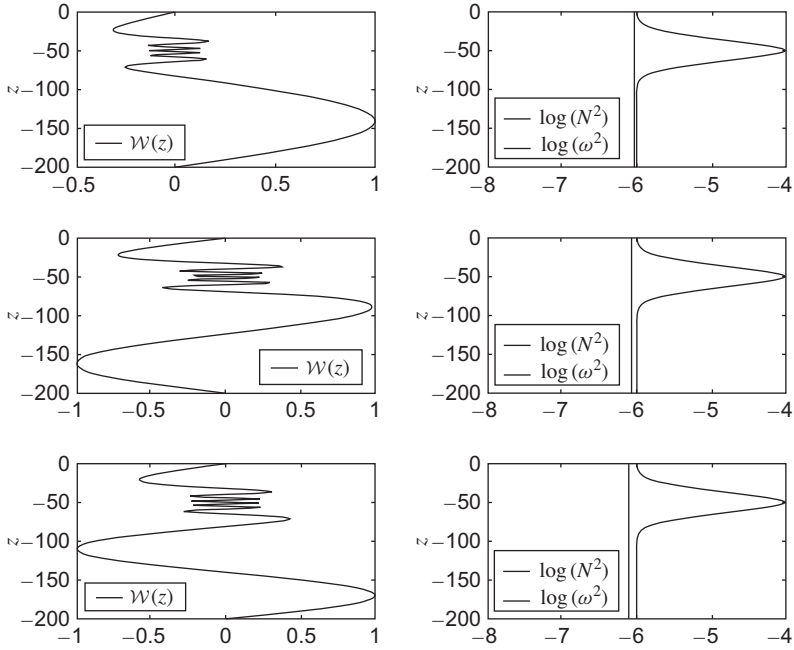

FIGURE 13.8 Modes 10–12 for the same nonuniform stratification as in the previous figure. Again, the left panel shows the vertical structure of the modes, whereas the right panel compares their ω^2 values to the N^2 values. Note the fine structure in the vicinity of the pycnocline and that the values of ω^2 fall below the minimum N^2 value.

twice across a peak in N^2, a pycnocline is accompanied by two turning points, one below and one above.

For higher modes (Fig. 13.8), ω^2 decreases and approaches the minimum of N^2. The turning points move away from the pycnocline until they disappear when, for high enough mode numbers, the corresponding ω^2 values fall below the N^2 minimum. Those higher modes have a structure that is oscillatory everywhere (Fig. 13.8). Surprisingly, amplitudes are now lowest near the pycnocline. This is due to the fact that the frequency difference is maximum ($\omega^2 - N^2$ largest) near the pycnocline, and resonant behavior is thus stronger away from the pycnocline, where the amplitude is consequently higher.

For even higher modes, the modal frequency ω approaches the inertial frequency f, and a new behavior emerges (Fig. 13.9). The regions above and below the pycnocline start to be decoupled, with one mode being almost entirely confined to one side of the pycnocline, the next mode to the other side, and so alternatively with mode number. The pycnocline appears to act as a barrier. In the limit of an extremely sharp pycnocline (very high N^2 peak), the

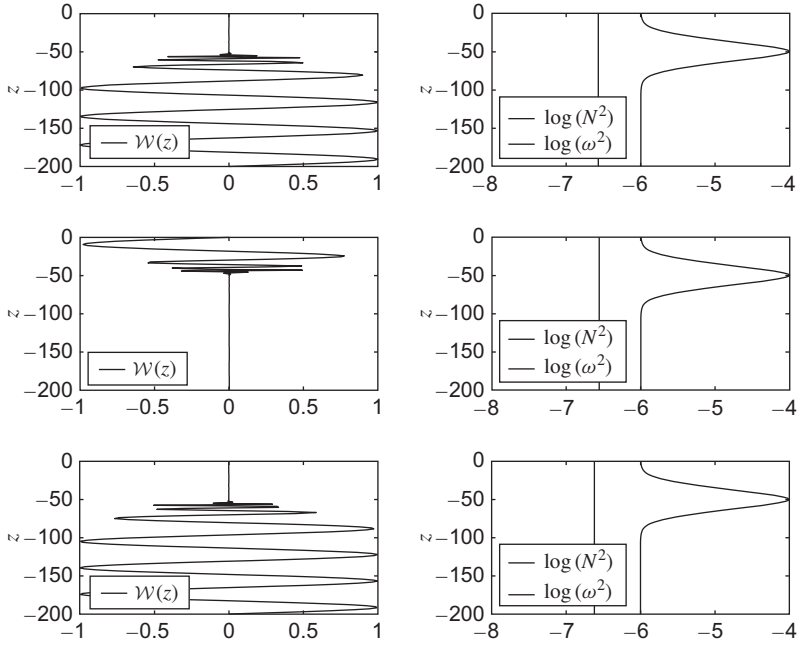

FIGURE 13.9 Modes 26–28 for the same nonuniform stratification as in the previous two figures. Again, the left panel shows the vertical structure of the modes, whereas the right panel compares their ω^2 values to the N^2 values. These modes, for which the frequencies approach the inertial frequency f, are almost entirely confined on one side or the other of the pycnocline. In other words, a pycnocline acts as a vertical barrier to near-inertial waves.

stratification effectively becomes a two-layer system, for which waves near the inertial frequency can exist in each layer independently of the other.

13.5 LEE WAVES

Internal waves in the atmosphere and ocean can be generated by a myriad of processes, almost wherever a source of energy has some temporal or spatial variability. Oceanic examples include the ocean tide over a sloping bottom, mixing processes in the upper ocean (especially during a hurricane), instabilities of shear flows, and the passage of a submarine. In the atmosphere, one particularly effective mechanism is the generation of internal waves by a wind blowing over an irregular terrain such as a mountain range or hilly countryside. We select the latter example to serve as an illustration of internal-wave theory because it has some meteorological importance and lends itself to a simple mathematical treatment.

To apply the previous linear-wave theory, we naturally restrict our attention to small-amplitude waves and, consequently, to small topographic irregularities.

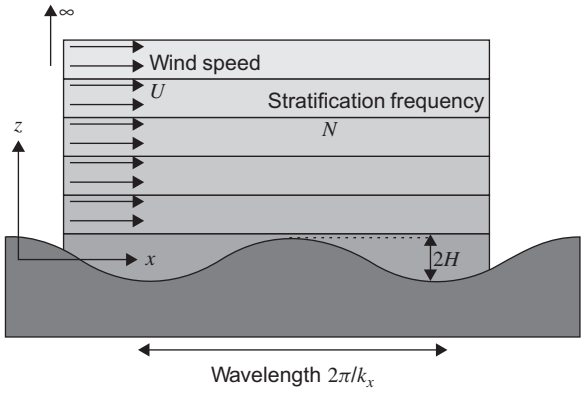

FIGURE 13.10 Stratified flow over a wavy terrain. The difference in elevation between crests and troughs is assumed small to justify a linear analysis. Then, the flow over any terrain configuration can be obtained from the superimposition of elementary wave solutions.

This restriction also permits us to study a single topographic wavelength, from which the principle of linear superposition should allow us to construct more general solutions. The model (Fig. 13.10) consists of a stratified air mass of uniform stratification frequency N flowing at speed U over a slightly wavy terrain. The ground elevation is taken as a sinusoidal function $b = H\cos k_x x$ of amplitude H (the trough-to-crest height difference is then $2H$) and wavenumber k_x (the wavelength is then $2\pi/k_x$). The wind direction (along the x-axis of the model) is chosen to be normal to the troughs and crests so that the problem is two-dimensional.

Because our theory has been developed for waves in the absence of a main flow, we translate the x-axis with the wind speed. The topography then appears to move at speed U in the negative x-direction:

$$\begin{aligned} z = b(x+Ut) &= H\cos[k_x(x+Ut)] \\ &= H\cos(k_x x - \omega t), \end{aligned} \tag{13.35}$$

where the frequency is defined as

$$\omega = -k_x U \tag{13.36}$$

and is a negative quantity. Because a particle initially on the bottom must remain there at all times (no airflow through the ground), a boundary condition is

$$w = \frac{\partial b}{\partial t} + u\,\frac{\partial b}{\partial x} \quad \text{at} \quad z = b, \tag{13.37}$$

which can be immediately linearized to become

$$\begin{aligned} w &= \frac{\partial b}{\partial t} \\ &= H\omega\sin(k_x x - \omega t) \quad \text{at} \quad z = 0, \end{aligned} \tag{13.38}$$

by virtue of our small-amplitude assumption.

The solution to the problem, which must simultaneously be of type (13.7) and meet condition (13.38), can be stated immediately:

$$u = k_z UH \sin(k_x x + k_z z - \omega t) \tag{13.39a}$$

$$w = -k_x UH \sin(k_x x + k_z z - \omega t) \tag{13.39b}$$

$$p' = -\rho_0 k_z U^2 H \sin(k_x x + k_z z - \omega t) \tag{13.39c}$$

$$\rho' = \frac{\rho_0 N^2 H}{g} \cos(k_x x + k_z z - \omega t), \tag{13.39d}$$

where the vertical wavenumber k_z is required to meet the dispersion relation (13.4):

$$k_z^2 = \frac{N^2}{U^2} - k_x^2. \tag{13.40}$$

The mathematical structure of this last expression shows that two cases must be distinguished: Either $N/U > k_x$ and k_z is real, or $N/U < k_x$ and k_z is imaginary. Note that solution (13.39) is formulated in the moving reference frame. To obtain the stationary solution in the fixed frame of the topography, one needs to add advection by the wind.

13.5.1 Radiating Waves

Let us first explore the former situation, which arises when the stratification is sufficiently strong ($N > k_x U$) or when the topographic wavelength is sufficiently long ($k_x < N/U$). Physically, the time $2\pi/k_x U$ taken by a particle traveling at the mean wind speed U to go from a trough to the next trough (i.e., up and down once) is longer than the natural oscillatory period $2\pi/N$, and internal waves can be excited. Solving Eq. (13.40) for k_z, we have two solutions at our disposal,

$$k_z = \pm\sqrt{\frac{N^2}{U^2} - k_x^2}, \tag{13.41}$$

but because the source of wave energy is at the bottom of the domain, only the wave with upward group velocity is physically relevant. According to Eqs. (13.10) and (13.36), we select the positive root.

The wave structure in the framework fixed with the topography (Fig. 13.11) is steady and such that all density surfaces undulate like the terrain, with no vertical attenuation but with an upwind phase tilt with height. The angle θ between the wave fronts (lines joining crests) and the vertical, which is also the angle between the wavenumber vector and the horizontal, is given by

$$\cos\theta = \frac{k_x U}{N}, \tag{13.42}$$

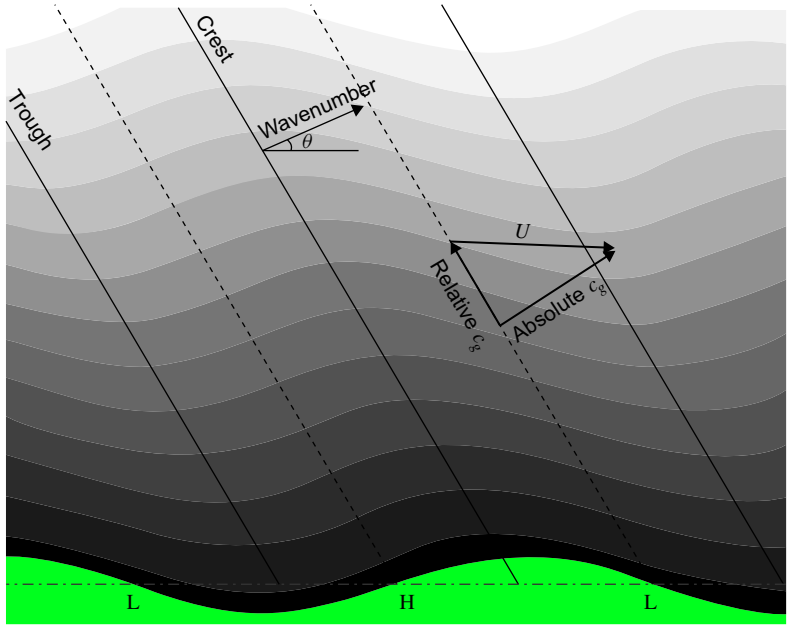

FIGURE 13.11 Structure of a mountain wave in the case of strong stratification or long wavelength ($k_x U < N$). Note the absence of vertical attenuation and the presence of a phase shift with height. The group velocity with respect to the ground is oriented upward and downwind. The pressure distribution, with highs on wind-facing slopes and lows on flanks in the wind's shadow, exerts a drag on the moving air mass.

so that $k_x = k\cos\theta$, $k_z = k\sin\theta$, with $k = \left(k_x^2 + k_z^2\right)^{1/2}$. The group velocity in the fixed frame is equal to the group velocity relative to the moving wind, given by Eq. (13.10) with $\omega = -k_x U$, plus the velocity U in the x-direction:

$$c_{gx} = -U\frac{k_z^2}{k^2} + U = U\cos^2\theta \tag{13.43}$$

$$c_{gz} = U\frac{k_x k_z}{k^2} = U\sin\theta\cos\theta. \tag{13.44}$$

It tilts upward as required, and its direction coincides with that of the wavenumber (Fig. 13.11). Energy is thus radiated upward and downwind. We shall not calculate the energy flux and will only show that the terrain exerts a drag force on the flowing air mass. The drag force, which is minus the Reynolds stress, is

$$\text{Drag force} = +\rho_0\,\overline{uw}\,|_{z=0} = -\frac{1}{2}\,\rho_0 k_x k_z U^2 H^2,$$

where the overbar indicates an average over one wavelength. The minus sign indicates a retarding force. The existence of this force is also related to the fact

that the high pressures are situated on the hill flanks facing the wind, and the lows are in the wind's shadow. Clearly, the wind faces a braking force.

13.5.2 Trapped Waves

The second case, leading to an imaginary value for k_z, occurs for weak stratifications ($N < k_x U$) or short waves ($k_x > N/U$). To avoid dealing with imaginary numbers, we define the quantity a as the positive imaginary part of k_z, that is, $k_z = \pm \mathrm{i}\, a$ with

$$a = \sqrt{k_x^2 - \frac{N^2}{U^2}}. \tag{13.45}$$

The solution now contains exponential functions in z, and the physical nature of the problem dictates that we retain only the function that decays away from the ground. In the reference framework translating with the wind speed U, the solution is

$$u = aUH\mathrm{e}^{-az}\ \cos(k_x x - \omega t) \tag{13.46}$$

$$w = -k_x UH\mathrm{e}^{-az}\ \sin(k_x x - \omega t) \tag{13.47}$$

$$p' = -\rho_0 aU^2 H\mathrm{e}^{-az}\ \cos(k_x x - \omega t) \tag{13.48}$$

$$\rho' = \frac{\rho_0 N^2 H}{g}\mathrm{e}^{-az}\ \cos(k_x x - \omega t). \tag{13.49}$$

The wave structure is depicted in Fig. 13.12. Density surfaces undulate at the same wavelength as the terrain, but the amplitude decays with height. There is no vertical phase shift. Because the waves are contained near the ground, in a boundary layer of thickness on the order of $1/a$, there is no upward energy radiation. The absence of such energy loss is corroborated by the absence of a drag force:

$$\text{Drag force} = +\rho_0 \overline{uw}\,|_{z=0} = 0.$$

The Reynolds stress vanishes because u and w are now in quadrature. Physically, the high pressures are in the valleys, the lows on the hilltops, and the pressure distribution causes no work against the wind.

13.6 NONLINEAR EFFECTS

All we have said thus far on internal waves is strictly applicable only if their amplitude is small, but internal-wave amplitudes can be quite large. For example, Liu et al. (2006) have observed internal waves in Luzon Strait (South China Sea) with amplitudes as high as 140 m.

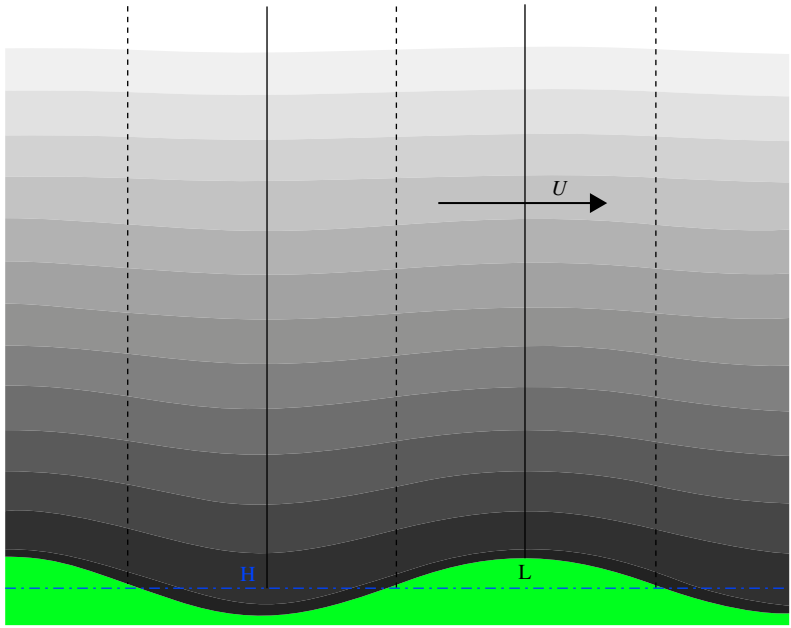

FIGURE 13.12 Structure of a mountain wave in the case of weak stratification or short wavelength ($N < k_x U$). Note the attenuation with height and the absence of vertical phase shift. The pressure distribution, with highs in valleys and lows on hill tops, causes no drag on the moving air mass.

The obvious question is: When do internal-wave dynamics become nonlinear? The answer lies in comparing the displacements of the particles caused by the wave to the wavelength: If those displacements are much shorter than the wavelength, then advective processes are unimportant, and the linear analysis is justified. The maximum horizontal displacement of fluid particles subject to an oscillatory horizontal velocity of the type $u = U\sin(k_x x + k_z z - \omega t)$ is U/ω, whereas the horizontal wavelength is $2\pi/k_x$. We thus require $U/\omega \ll 2\pi/k_x$, or because of Eq. (13.4),

$$U \ll \frac{2\pi N}{\sqrt{k_x^2 + k_z^2}} \leq \frac{2\pi N}{k_z}.$$

Since $2\pi/k_z$ is the vertical wavelength, which we can take as the depth scale of the motion and denote by H, the criterion becomes

$$Fr = \frac{U}{NH} \ll 1. \tag{13.50}$$

Thus, the preceding description of internal waves is applicable only to situations where the Froude number (based on the wave-induced velocities and the

vertical wavelength) is much less than unity. Note that NH is approximately the horizontal phase speed of the wave, and the criterion can be interpreted as a restriction to fluid velocities much smaller than the wave speed. When the preceding condition is not met, nonlinear effects cannot be neglected, and the spectral analysis fails.

A first possible effect is wave breaking. The crest (or trough) overtakes the rest of the wave, and the wave rolls over not unlike the surf on the sea surface on approaching a beach. This type of instability, due to the wave motion itself, is termed *advective instability*. At lower energy levels, waves do not overturn but may nonetheless be sufficiently strong not to conform to the linear theory. Wave interactions create harmonics, and energy spreads over a continuous spectrum, usually spanning several decades in frequencies and wavenumbers.

Observed spectra in the deep ocean (i.e., in areas remote from important topographic influences) all show a striking resemblance (Munk, 1981), suggesting the existence of a universal spectrum. This observation led Christopher J. R. Garrett and Walter H. Munk to formulate in 1972 a prototypical spectrum for internal-wave energy. This model spectrum was subsequently modified and refined (Garrett & Munk, 1979; Munk, 1981) and has become known as the *Garrett–Munk spectrum*. The expression for the spectral energy density is

$$E(k,m) = \frac{3fN\mathrm{E}\, m\, m_*^{3/2}}{\pi (m+m_*)^{5/2}\, (N^2k^2+f^2m^2)}, \tag{13.51}$$

where $k = \sqrt{k_x^2+k_y^2}$ is the horizontal wavenumber, $m = k_z$ the vertical wavenumber, m_* a reference wavenumber to be determined from observations, and E a dimensionless constant setting the overall energy level (see Fig. 13.13).

The Garrett–Munk spectrum is largely empirical in the sense that its formulation is based on observations, simple dimensional considerations, and elementary physics. Yet, it has been shown to conform to a large number of observations, prompting the conjecture (Munk, 1981) that the internal-wave climate in the deep ocean is somehow regulated by a saturation process rather than by external generation processes. Lvov and Tabak (2001) have advanced a theory that closely but not exactly reproduces the Garrett–Munk spectrum.

In coastal areas, where topographic irregularities play a dominant role in generating internal waves, it is not unusual to find coherent wave groups at a single (tidal) frequency. Under certain conditions, the dispersion effect (different wave speeds for different wavenumbers) can annihilate the nonlinear steepening effect (crests or troughs overtaking the rest of the wave), yielding a robust wave called *internal solitary wave* (Turner, 1973, Chapter 3). Figure 13.2 displays the surface signature of a train of internal solitary waves.

Theory, field observations, and laboratory simulations indicate that internal-wave characteristics are substantially altered in the presence of shear flows. Although a general theory is beyond our present scope, it is worth noting that, like waves in a laterally sheared flow of a homogeneous fluid, internal waves can

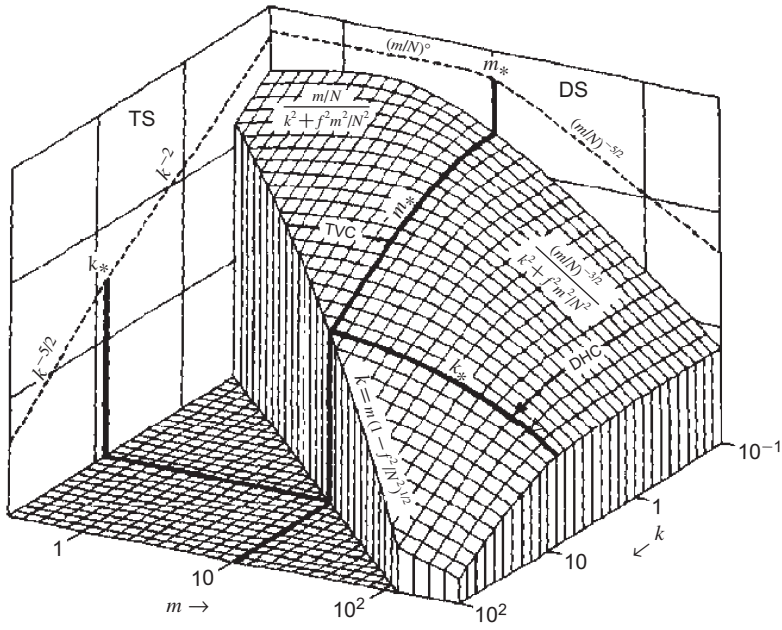

FIGURE 13.13 Universal spectrum of internal waves in the ocean, according to Garrett and Munk (1979). The spectral energy density E is plotted as a function of k and m, the horizontal and vertical wavenumbers, respectively. The two-dimensional spectrum can be integrated over one or the other of its variables to obtain the "towed spectrum" (TS) or the "dropped spectrum" (DS).

also encounter critical levels in a vertically sheared flow (wave speed equal to local flow velocity).

For weak-to-moderate shear flows ($\mathrm{d}u/\mathrm{d}z < 2N$) in nonrotating (Booker & Bretherton, 1967) and rotating (Jones, 1967) stratified fluids, theoretical considerations show that on approaching a critical level, the internal-wave vertical wavenumber increases without limit and the group velocity becomes horizontal, thus aligning itself with the flow. The theory also shows that the time taken for the energy to reach the critical level is infinite, implying that dissipative effects become important. Physically, the energy is not focussed and amplified but absorbed and dissipated at the critical level.

In stronger shear flows ($\mathrm{d}u/\mathrm{d}z > 2N$), instabilities develop. This *shear instability*, treated in the following chapter, is the vertical analogue of the barotropic instability in horizontally sheared flows (Chapter 10).

ANALYTICAL PROBLEMS

13.1. In a coastal ocean, the water density varies from 1028 kg/m^3 at the surface to 1030 kg/m^3 at depth of 100 m. What is the maximum internal-wave frequency? What is the corresponding period?

13.2. Internal waves are generated along the coast of Norway by the M_2 surface tide (period of 12.42 h). If the stratification frequency N is $2 \times 10^{-3}\ \mathrm{s}^{-1}$, at which possible angles can the energy propagate with respect to the horizontal? (*Hint*: Energy propagates in the direction of the group velocity.)

13.3. Derive the dispersion relation of internal gravity waves in the presence of rotation, assuming $f < N$. Show that the frequency of these waves must always be higher than f but lower than N. Compare vertical phase speed to vertical group velocity.

13.4. A 10-m/s wind blows over a rugged terrain, and lee waves are generated. If the stratification frequency is equal to $0.03\ \mathrm{s}^{-1}$ and if the topography is approximated to a sinusoidal pattern aligned perpendicularly to the wind, with a 25-km wavelength and a height difference from trough to crest of 500 m, calculate the vertical wavelength, the angle made by the wave fronts (surfaces of constant phase) with the horizontal, and the maximum horizontal velocity at the ground. Also, where is this maximum velocity observed (at crests, at troughs, or at the points of maximum slope)?

13.5. A 75-km/h gale wind blows over a hilly countryside. If the terrain elevation is approximated by a sinusoid of wavelength 4 km and amplitude of 40 m and if the stratification frequency of the air mass is $0.025\ \mathrm{s}^{-1}$, what are the vertical displacements of the air particles at 1000 m and 2000 m above the mean ground level?

13.6. Determine the kinetic and potential energy densities of a pure internal wave.

13.7. Demonstrate that a single internal wave satisfying the dispersion relation is not only solution of the linearized perturbation equations but also of the fully nonlinear equations. What happens if two waves are present in the system?

13.8. Study internal waves in a stratified system of stratification frequency $N(z)$ in a vertically bounded domain using the hydrostatic approximation in Eq. (13.12). Show that the separation constant now appears as the eigenvalue to be calculated and that the associated radius of deformation no longer depends on the horizontal wavenumber squared $k_x^2 + k_y^2$.

13.9. Search for the existence of an internal Kelvin wave by using the separation-of-constants approach. Use the long-wave (or hydrostatic) assumption adapting Eq. (13.12) as necessary. Particularize to the case of uniform N^2.

13.10. Consider Skjomen Fjord near Narvik in northern Norway, with length L of 25 km, average depth H of about 110 m, and stratification frequency N

of about 2.0×10^{-3} s^{-1}. What are the lowest two frequencies of internal waves with wavelength equal to the fjord's length?

13.11. Despite the fact that system (13.2) has four time derivatives, we obtained a dispersion relation that yields only a pair of eigenfrequencies. Can you resolve the paradox?

NUMERICAL EXERCISES

13.1. Use the dispersion relation of pure internal waves (13.4) to illustrate the superposition of two waves by an animation in the (x, z) plane of size L_x, H. Can you see the group velocity when using two waves of equal amplitude and the two wavenumber vectors $(k_x = 35/L_x, k_z = 10/H)$ and $(k_x = 40/L_x, k_z = 12/H)$?

13.2. For the matrices and eigenvalues of problem (13.33), prove that

$$\lambda_{\min} \leq \frac{\mathbf{x}^{\mathsf{T}}\mathbf{B}\mathbf{x}}{\mathbf{x}^{\mathsf{T}}\mathbf{C}\mathbf{x}} \leq \lambda_{\max}. \tag{13.52}$$

To prove these so-called Rayleigh–Ritz inequalities Eq. (13.52) for symmetric positive definite matrices $\mathbf{B}$ and $\mathbf{C}$,

- assume that all eigenvalues are different,
- demonstrate that $\left(\mathbf{w}^i\right)^{\mathsf{T}} \mathbf{B}\mathbf{w}^j = \delta_{ij}$ and $\left(\mathbf{w}^i\right)^{\mathsf{T}} \mathbf{C}\mathbf{w}^j = \delta_{ij}$,
- prove that all eigenvectors $\mathbf{w}^i$, $i = 1, \ldots$. are linearly independent, and
- write any vector $\mathbf{x}$ as a weighted sum of those independent vectors, and use this expression in the Rayleigh–Ritz quotient to prove the Rayleigh–Ritz inequalities.

Adapt the code `iwave.m` to provide estimates of the upper and lower bound using a series of random vectors $\mathbf{x}$ to calculate the Rayleigh–Ritz estimator $(\mathbf{x}^{\mathsf{T}}\mathbf{B}\mathbf{x})/(\mathbf{x}^{\mathsf{T}}\mathbf{C}\mathbf{x})$ and store the minima and maxima of the calculated quotient. Seek how the bounds become increasingly precise as you choose additional random vectors.

13.3. By substitution of $\omega^2 = (1 + \tilde{\lambda})f^2$ into Eq. (13.32) and redefining $\mathbf{B}$, show that all eigenvalues ω_i satisfy $\omega_i^2 \geq f^2$. Incidentally show that you can recast the problem into a standard eigenvalue problem.
By substitution of $\omega^2 = (1 - \tilde{\lambda})N_{\max}^2$ into Eq. (13.32) and redefining $\mathbf{B}$, show that all eigenvalues ω_i satisfy $\omega_i^2 \leq N_{\max}^2$.

13.4. Adapt `iwavemed.m` to read temperature and salinity profiles from oceanographic data bases, such as the Levitus climatology,[4] and calcu-

[4] See http://www.cdc.noaa.gov/cdc/data.nodc.woa94.html.

late the radius of deformation for the Gulf Stream region. To read a climatological atlas, you can use `levitus.m` and select a location.

13.5. Assess numerically the convergence rate for eigenvalues and eigenfunctions in the case of uniform stratification by adapting `iwave.m`.

13.6. Discretize the eigenvalue problem of the sheared-flow instability (10.9) using the same techniques as in Section 13.4.4. What can you say about the positive-definite nature of the matrices involved? Try finding the numerical eigenvalues and growth rates of profiles you think are probably unstable in Analytical Problem 10.2.

Walter Heinrich Munk
1917–

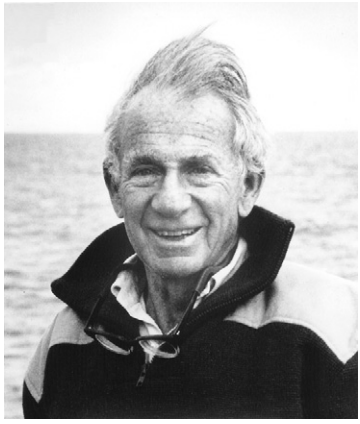

Born in Austria and educated in the United States, Walter Heinrich Munk became interested in oceanography during a summer project under Harald Sverdrup at the Scripps Institution of Oceanography and quickly developed a fascination for ocean waves. This interest in waves arose partly because of the wartime need to predict sea and swell and also because Munk found wave research a challenge of intermediate complexity between simple periodic oscillations and hopeless chaos. As years went by, Munk eventually investigated all wavelengths, from the small capillary waves responsible for sun glitter to the ocean-wide tides. His studies of internal waves, in collaboration with Christopher Garrett, led him to propose a universal spectrum for the distribution of internal-wave energy in the deep ocean, now called the Garrett–Munk spectrum. More recently, pursuing an interest in acoustic waves, Munk initiated ocean tomography, a method for determining the large-scale temperature structure in the ocean from the measure of acoustic travel times. (*Photo by Jeff Cordia*)

Adrian Edmund Gill
1937–1986

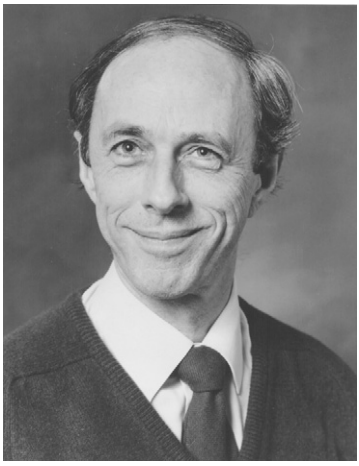

Born in Australia, Adrien Edmund Gill pursued his career in Great Britain. His publications spanned a wide range of topics, including wind-forced currents, equatorially trapped ocean waves, tropical atmospheric circulation, and the El Niño–Southern Oscillation phenomenon, and culminated in his treatise *Atmosphere-Ocean Dynamics* (Gill, 1982). His greatest contributions relied on the formulation of simple yet illuminating models of geophysical flows. It has been said (only half jokingly) that he could reduce all problems to a simple ordinary differential equation with constant coefficients, with all the essential physics retained. Although he never held a professorship, Gill supervised numerous students at the Universities of Cambridge and Oxford. He is also remembered for his unassuming style and for the generosity with which he shared his ideas with students and colleagues. (*Photo credit: Gillman & Soame, Oxford*)